NASA Contractor Report 182120

# On Governing Equations for Crack Layer Propagation



A. Chudnovsky and J. Botsis
*University of Illinois at Chicago Circle*
*Chicago, Illinois*

April 1988

Prepared for
Lewis Research Center
Under Grant NAG3-754

National Aeronautics and
Space Administration

# I. INTRODUCTION

## Objectives

This project was set to examine the evolution of damage density and active zone of a crack layer (CL) under different fatigue loading histories in a model material. The effect of damage on the near crack tip stress field was studied by employing a newly developed technique of semi-empirical stress analysis.

## Achievements

- On the basis of the observed damage growth, we tested the basic hypothesis of the crack layer theory, i.e., a self-similarity of damage distribution in process of crack layer propagation.
- A new semi-empirical crack tip stress analysis, based on experimental measurements of the discontinuity density and the double layer potential technique, has been developed as a solution of crack-damage interaction problem. Evaluation of the stress intensity factor illustrates the methodology. This illustrative example suggests an alternative to the Dugdale-Barenblatt model.
- The first step in construction of the CL constitutive relationship has been made.

Analysis of the experimental results showed that Arrhenius type constitutive relationship describes very well the expansion of the active zone.

In three consecutive parts we describe our findings. This work is being prepared for publication:

(a) J. Botsis and B. Kunin, 'On Self-Similarity of Crack Layer,' Intern. J. Fracture, to appear.

(b) A. Chudnovsky and M. Ben Onenzdon, 'Semi-Empirical Crack Tip Analysis,' Intern, J. Fracture, to appear.

(c) J. Botsis and A. Chudnovsky, 'On the Expansion of Active Zone of a Crack Layer,' to be published.

## I. DAMAGE ANALYSIS OF A RECTILINEAR CRACK LAYER

Early results of investigations in this program showed that fracture propagates as a crack surrounded by a layer of damage, namely, a CL. A well developed CL in our model material is shown in Fig. 1a.

The self-similarity hypothesis states that the value of the damage density $\rho$ at a point $\underline{x}$ of the active zone at a time $t$ coincides with that at the corresponding point in the initial ($t = 0$) configuration of the active zone, the correspondence being given by a time-dependent affine transformation of the space variables

$$\rho_t(\underline{x}) = \rho_o(A_t \cdot (\underline{x} - \underline{\ell}_t)) \ , \tag{I.1}$$

where $\rho_t(\underline{x})$ is the value of the damage parameter at the point $\underline{x}$ at the time $t$, $\rho_o = \rho_t\big|_{t=0}$, $A_t$ is a time-dependent 2x2 matrix for a plane problem ($A_t\big|_{t=0}$ being the identity matrix), and $\underline{\ell}_t$ is the position of the crack tip at the time $t$ ($\underline{\ell}_t\big|_{t=0} = 0$). Note that, as any matrix, $A_t$ can be uniquely decomposed as a product of three time-dependent matrices: a scalar matrix (expansion of the active zone), a symmetric positive definite matrix whose determinant equals one (distortion of the active zone), and an orthogonal matrix (rotation of the active zone). The above formulation of 'self-similarity' is contained in [I.1] in its infinitesimal form.

The requirement (1) has two major implications. i) It reduces the evolution of the <u>function</u> $\rho(\underline{x})$ to the evolution of six <u>scalar</u> parameters: four components of the matrix $A_t$ and two components of the vector $\underline{\ell}_t$. ii) It allows to express the energy release rates associated with the translation rotation, and expansion of the active zone (the 'driving forces' in the terminology of [I.1]) in the form of the well-known J, L an M integrals,

respectively [I.4]. The corresponding energy release rate for active zone distortion has a similar integral representation [I.1,2].

A complete examination of the self-similarity hypothesis would require comparison of damage distribution within the active zone at different instances of its evolution. However, such complete data is not available at present. Instead, available is damage distribution within a well developed CL.

Notice that, at any instance $t$, the trailing edge is the only portion of the active zone along which the damage parameter will remain unaltered as tne CL continues to evolve.

For this reason we examine the implications of the self-similarity hypothesis for the evolution of damage distribution along the trailing edge. The latter is approximated by a straight segment perpendicular to the crack path.

Due to the symmetry of the loading-specimen geometry and the homogeneity of the material, (a) the crack follows the straight path along along $x_1$-axis, (b) there is no rotation of the active zone, hence $A_t$ is a symmetric matrix, (c) the principal axes of $A_t$ coincide with the coordinate axes $x_1$, $x_2$ (Fig. I.1). Thus at a time $t$ the position $\underline{\ell}_t$ of the crack tip, the generic point $\underline{x}$ of the trailing edge and the matrix $A_t$ have the form

$$\underline{\ell}_t = \begin{pmatrix} \ell(t) \\ 0 \end{pmatrix} , \quad \underline{x} = \begin{pmatrix} \ell(t) \\ x_2 \end{pmatrix} , \quad A_t = \begin{pmatrix} a_1(t) & 0 \\ 0 & a_2(t) \end{pmatrix} , \tag{I.2}$$

Taking (I.2) into account, equation (I.1) for the points of the trailing edge reduces to

$$\rho_t(\ell(t),x_2) = \rho_o(0,a_2(t)x_2) . \tag{I.3}$$

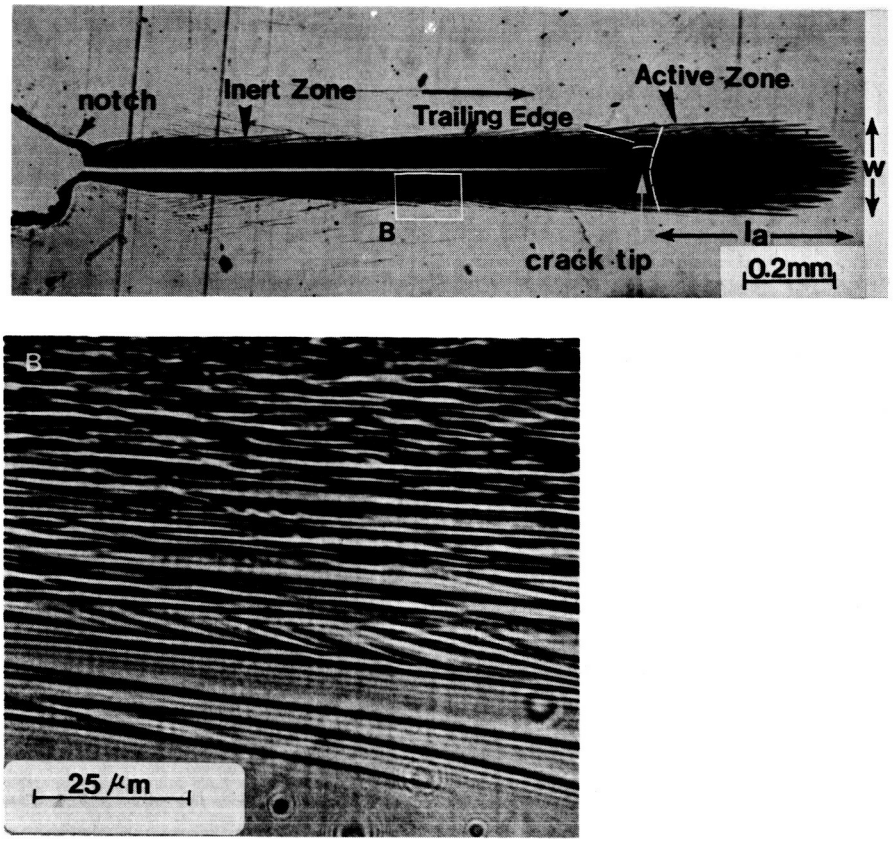


Fig. I.1 (a) General view of a CL in polystyrene. (b) Higher magnification of the boxed area B after thinning.

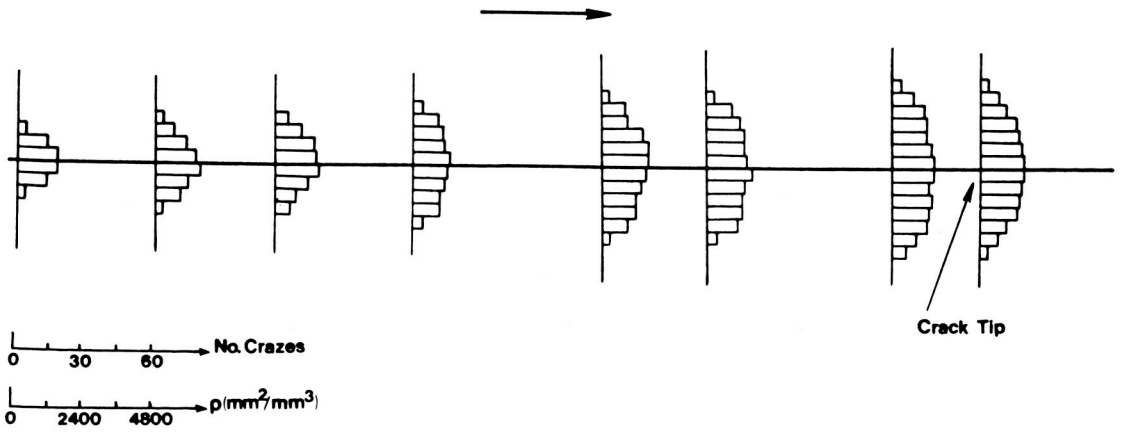


Fig. I.2 Histograms of craze distribution for eight cross sections within the inert zone of a CL.

Equation (I.3) implies that, for any two positions of the trailing edge, the corresponding along-the-trailing edge damage distributions are related by scaling (in $x_2$-direction).

This restricted form of the self-similarity hypothesis was tested using data on crazing distribution in a CL grown under fatigue in polystyrene loading [I.6]. Quantitative damage analysis was carried out on a thinned specimen employing optical microscopy and principles of quantitative stereology [I.5]. A micrograph of a typical portion of the CL is shown in Fig. I.1b. Details on the experimental procedures can be found in [I.6].

Figure I.2 represents the histograms of craze distribution in vertical cross sections at eight locations along the crack path. As a result of the present symmetry, the odd central moments of damage distributions in the vertical cross sections are negligibly small. As simplest indicators of whether the shape of the craze distribution stays the same <u>up to a uniform dilation</u> from section to section, we take the following two: a) the ratio of the total amount of crazes for a cross section to six times the standard deviation of the damage distribution for the same cross section (this is, for practical purposes, the average damage density in the cross section); b) the ratio of the variance of the cross-sectional damage distribution to the square root of its fourth central moment. Both ratios are independent of scaling and thus should remain constant, if 'self-similarity' holds.

Figure I.3 (I.4) represents the values of the first (second) of the above ratios for the eight aforementioned sections. From the data in Figs. I.3 and I.4, we conclude that both ratios stay constant to within experimental error.

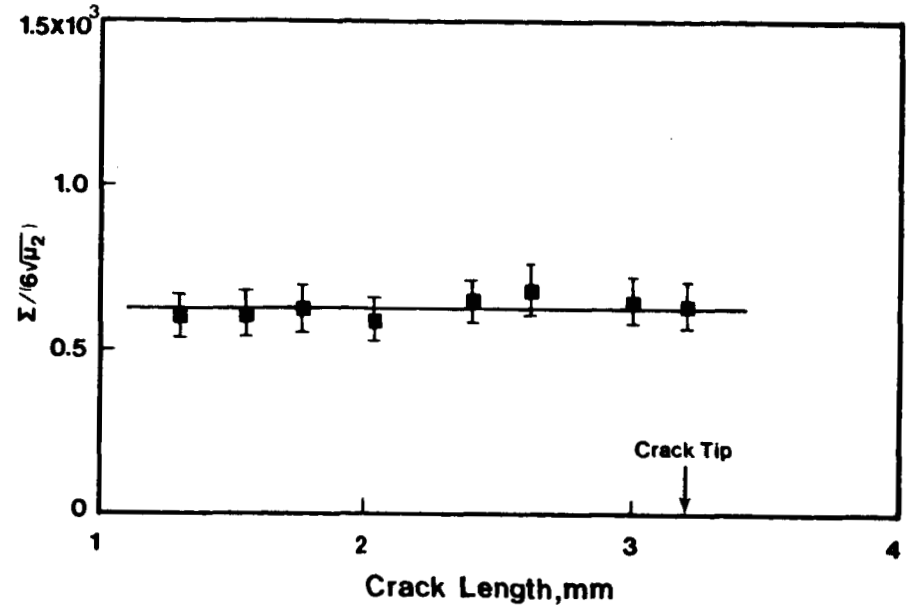


Fig. I.3 For each of the eight cross-sectional craze distributions from Fig. I.2, the 'average craze density' is shown; here $\Sigma$ is the total number of crazes in a cross section, $\sqrt{\mu_2}$ is the standard deviation of the craze distribution in the same cross section.

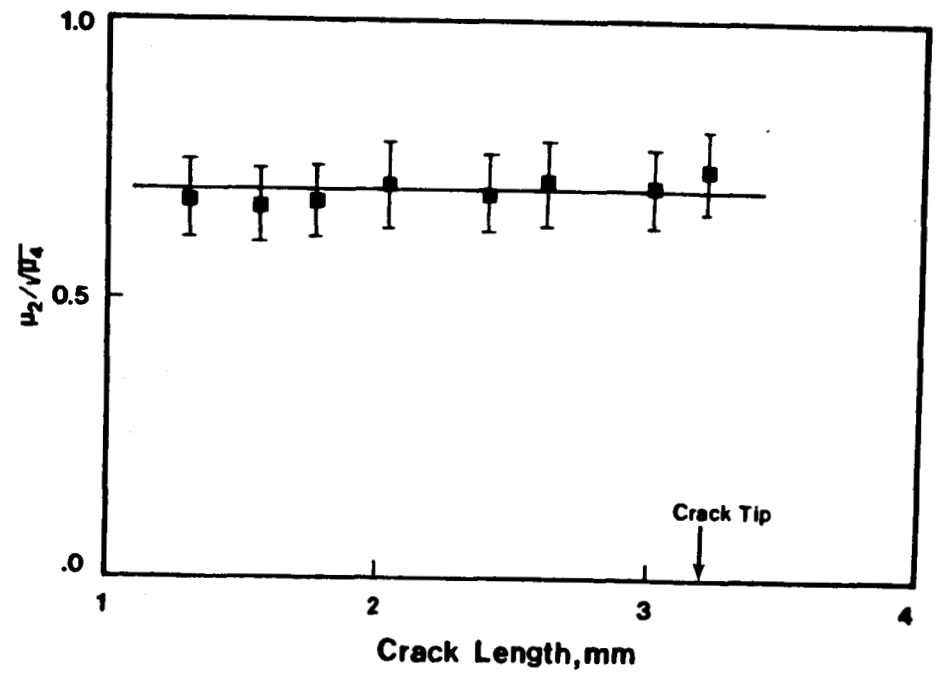


Fig. I.4 For each of the distributions (Fig. I.2), the ratio of its variance $\mu_2$ to the square root of its fourth central moment $\sqrt{\mu_4}$ is shown.

## REFERENCES


[I.1] A. Chudnovsky, 10th U.S. National Congress on Applied Mechanics, Austin, Texas (1986), also to appear in Journal of Applied Mechanics.

[I.2] A. Chudnovsky, 'Crack Layer Theory,' NASA Contractors Report No. 174634.

[I.3] J. Botsis, A. Chudnovsky and A. Moet, International Journal of Fracture, 33 (1987), pp. 263-276.

[I.4] B. Budiansky and J. Rice, Journal of Applied Mechanics, 40 (1973), pp. 201-203.

[I.5] E. E. Underwood, 'Quantitative Stereology,' Addison-Wesley, New York, NY (1970).

[I.6] J. Botsis, 'Damage Analysis of a Crack Layer,' Submitted to Journal of Material Science.

# II. SEMI-EXPERIMENTAL STRESS ANALYSIS

## 1. Introduction

Determination of near and far fields for a crack surrounded by an array of microcracks is a key problem for modelling of crack propagation and stability. We approach this problem in two steps: at first a multiple crack interaction is characterized experimentally in terms of Crack Opening Displacements (CODs). Then, as a second step, we reconstruct the displacement, strain and stress fields by analytical means employing the results of the first step.

The problem of multiple crack interaction has been recently addressed by various authors (a brief review can be found in [II.1-3]). This problem can be expressed formally as a system of singular integral equations with respect to unknown CODs. These equations represent the boundary conditions on the surfaces of the cracks. Constructive solutions of the problem have been formulated for just a few types of crack configurations. In general, for a random configuration of a large number of microcracks the solution implies extremely tedious and time-consuming numerical procedure [II.4-6].

In this section, we employ experimentally observed COD's as the solution of the multiple crack interaction problem. Then the near and far fields will be reconstructed by means of the double layer potential technique. The foundation of the analysis is outlined in the second section and the evaluation of an effective Stress Intensity Factor (SIF) reflecting crack-microcrack interaction is presented in the third section as an illustrative example.

## 2. Formulation of a Semi-Empirical Analysis

Let us consider a microcrack of length $2\ell$ at a distance $\underset{\sim}{\xi}$ from the main crack tip (Fig. II.1). In this work, we assume plane stress; the case of

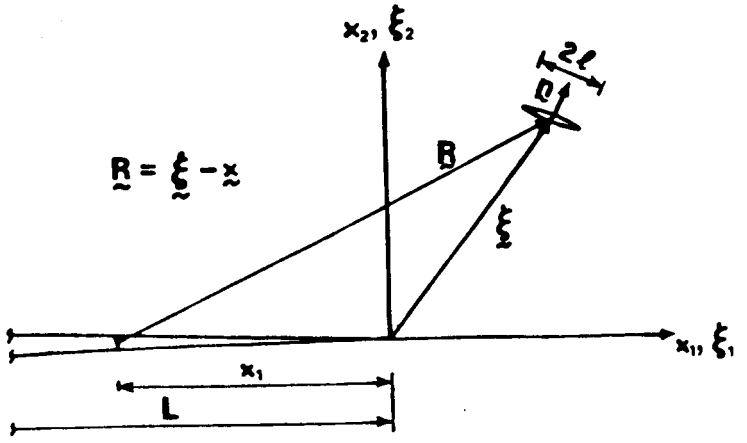


Fig. II.1 A single microcrack near a main crack, illustrating the coordinate system employed.

plane strain can be treated similarly. The microcrack is characterized as a discontinuity $\underset{\sim}{b}(\underset{\sim}{\xi})$, i.e., COD (double layer potential). As a result, it induces an additional opening displacement on the main crack. Adopting the symbols of the previous work of Chudnovsky, et al. [II.6-8], we express the displacement field $\underset{\sim}{u}(\underset{\sim}{x})$ generated by a microcrack as

$$\underset{\sim}{u}_{mic}(\underset{\sim}{x}) = \int_{\omega} \underset{\sim}{b}(\underset{\sim}{\xi})\ \underset{\sim}{\underset{\sim}{\Phi}}(\underset{\sim}{\xi},\underset{\sim}{x})\ d\underset{\sim}{\xi} \tag{II.1}$$

where $\omega$ is the microcrack line (surface in 3-D) and $\underset{\sim}{\underset{\sim}{\Phi}}(\underset{\sim}{\xi},\underset{\sim}{x})$ is the second Green's tensor which is defined as the displacement response at the point $\underset{\sim}{x}$ due to a unit discontinuity at the point of discontinuity $\underset{\sim}{\xi}$ (Fig. II.1). For example, in plane stress, the second Green's tensor for an infinite plane is given by (see, e.g., [I.8])

$$\underset{\sim}{\underset{\sim}{\Phi}}(\underset{\sim}{\xi},\underset{\sim}{x}) = -\frac{(1+\nu)}{4\pi R^2}\left[\frac{1-\nu}{1+\nu}\left(\underset{\sim}{n}_{\xi}\underset{\sim}{R} - \underset{\sim}{\underset{\sim}{R}}\underset{\sim}{n}_{\xi} + \underset{\sim}{n}_{\xi}\underset{\sim}{R}\underset{\sim}{\underset{\sim}{I}}\right) + 2\frac{\underset{\sim}{n}_{\xi}\underset{\sim}{R}}{R^2}\underset{\sim}{\underset{\sim}{R}}\underset{\sim}{R}\right] \tag{II.2}$$

where $\underset{\sim}{n}_\xi$ is the unit normal vector to the line (surface) across which the discontinuity takes place, $\nu$ is Poisson's ratio, I is the unit second rank tensor and R is the position vector, i.e., $\underset{\sim}{R} = \underset{\sim}{\xi} - \underset{\sim}{x}$ (Fig. II.1).

The displacement $\underset{\sim}{u}_A$ at an arbitrary point $\underset{\sim}{x}$ caused by a Microcrack Array (MA) is the sum of the displacements generated by each microcrack, i.e.,

$$\underset{\sim}{u}_A(\underset{\sim}{x}) = \sum_{k=1}^{N} \underset{\sim}{u}^{(k)}_{mic}(\underset{\sim}{x}) = \sum_{k=1}^{N} \int_{\omega^{(k)}} \underset{\sim}{b}^{(k)}(\underset{\sim}{\xi}) \underset{\sim}{\Phi}(\underset{\sim}{\xi}, \underset{\sim}{x})\, d\underset{\sim}{\xi} \qquad \text{(II.3)}$$

where N is the total number of microcracks in the array. If the size of the microcracks is small in comparison with the domain of the array and the number N of microcracks is sufficiently large, the summation in Eq. (II.3) can be substituted by integration of an appropriately introduced microcrack density over the array domain. Let us introduce a mesh within the domain (Fig. II.2a) and consider a typical square (with an area $A_{\alpha\beta} = \Delta\xi_{1\alpha}\Delta\xi_{2\beta}$) which contains $N_{\alpha\beta}$ microcracks (Fig. II.2b). Then the displacement vector due to the MA can be written as

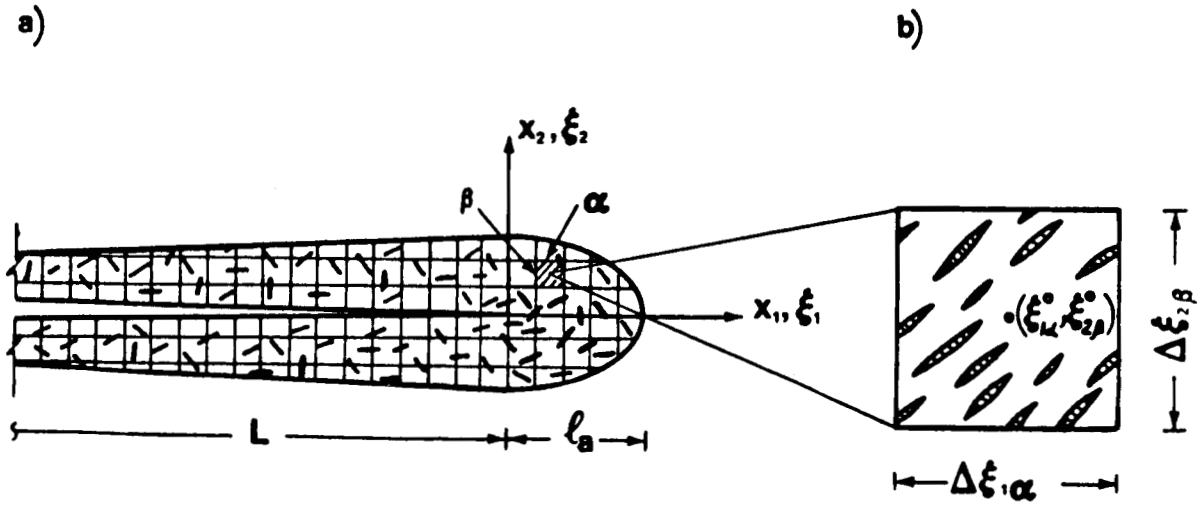


Fig. II.2a Schematic representation of the Microcrack Array (MA) surrounding the main crack and the subdivision of the domain into a rectilinear mesh.

Fig. II.2b A typical square for the determination of microcrack opening density.

$$\underset{\sim}{u}_A(\underset{\sim}{x}) = \sum_{\alpha=1}^{N_1} \sum_{\beta=1}^{N_2} \sum_{k=1}^{N_{\alpha\beta}} \int_{\omega^{(k)} \in A_{\alpha\beta}} \underset{\sim}{b}^{(k)}(\underset{\sim}{\xi}) \underset{\sim}{\Phi}(\underset{\sim}{\xi}, \underset{\sim}{x}) \, d\underset{\sim}{\xi} \tag{II.4}$$

where $N_1$ and $N_2$ are the numbers of rows and columns in the mesh, respectively. For infinitesimal squares, $|\xi - x|$ is much larger than the maximum of $|\Delta\xi|$, then $\underset{\sim}{\Phi}(\underset{\sim}{\xi}, \underset{\sim}{x})$ can be approximated by $\Phi(\xi^o_{1\alpha}, \xi^o_{2\beta}, \langle \underset{\sim}{n} \rangle_{\alpha\beta}, \underset{\sim}{x})$, in which $\xi^o_{1\alpha}$ and $\xi^o_{2\beta}$ are the coordinates of the center of the square and $\langle \underset{\sim}{n} \rangle_{\alpha\beta}$ is an average orientation of the microcracks within the square (Fig. II.2b). Then using the mean value theorem, Eq. (II.4) can be rewritten as

$$\underset{\sim}{u}_A(\underset{\sim}{x}) = \sum_{\alpha=1}^{N_1} \sum_{\beta=1}^{N_2} \underset{\sim}{c}(\xi^o_{1\alpha}, \xi^o_{2\beta}) \underset{\sim}{\Phi}(\xi^o_{1\alpha}, \xi^o_{2\beta}, \langle \underset{\sim}{n} \rangle_{\alpha\beta}, \underset{\sim}{x}) \Delta\xi_{1\alpha} \Delta\xi_{2\beta} \tag{II.5}$$

where the vector $\underset{\sim}{c}$ represents the microcrack opening density

$$\underset{\sim}{c}(\xi^o_{1\alpha}, \xi^o_{2\beta}) = (\Delta\xi_{1\alpha} \Delta\xi_{2\beta})^{-1} \sum_{k=1}^{N_{\alpha\beta}} \int_{\omega^{(k)} \in A_{\alpha\beta}} \underset{\sim}{b}^{(k)}(\underset{\sim}{\xi}) \, d\underset{\sim}{\xi} \tag{II.6}$$

This can be measured directly as the ratio of the area of the opened cracks within a square (shadowed area in Fig. II.2b) and the area of the square. The sum in Eq. (II.5) becomes an integral over the entire domain of the MA after an obvious limiting procedure ($|\Delta\xi| \to 0$, $N \to \infty$):

$$\underset{\sim}{u}_A(\underset{\sim}{x}) = \int_{V_A} \underset{\sim}{c}(\underset{\sim}{\xi}) \underset{\sim}{\Phi}(\underset{\sim}{\xi}, \langle \underset{\sim}{n} \rangle, \underset{\sim}{x}) \, d\underset{\sim}{\xi} \tag{II.7}$$

where $V_A$ represents the volume of the MA domain. The corresponding stress field $\sigma_A(x)$ induced by the microcracks array interacting with the main crack is presented as

$$\underset{\sim}{\sigma}_A(\underset{\sim}{x}) = \underset{\sim}{T}_x \int_{V_A} \underset{\sim}{c}(\underset{\sim}{\xi}) \underset{\sim}{\Phi}(\underset{\sim}{\xi}, \langle \underset{\sim}{n} \rangle, \underset{\sim}{x}) \, d\underset{\sim}{\xi} \tag{II.8}$$

where $\underset{\sim}{T}_x$ is the stress operator which transforms the displacement field $u_k$ into stress $\sigma_{ij}$

$$\sigma_{ij} = T_{ijk}u_k \; ; \quad T_{ijk} = \mu(\delta_{ik}\partial_j + \delta_{jk}\partial_i) + \lambda\delta_{ij}\partial_k \tag{II.9}$$

Here $\mu$ and $\lambda$ are Lame's constants, $\delta_{ij}$ is the Kronecker's delta (i,j = 1,2) and k = 1,2,3. The subscript x in (II.8) indicates that the differentiation in (II.9) is to be performed with respect to x.

## 3. An Illustrative Example: Evaluation of the SIF

In this section we evaluate the SIF at the crack tip caused by combination of the externally applied stress $\sigma_\infty$ and the MA induced stress $\sigma_A$. This particular example is suggested and closely related to the experimental observation of an array of crazes preceding and surrounding fatigue crack in polystyrene (Fig. II.3) [II.9].

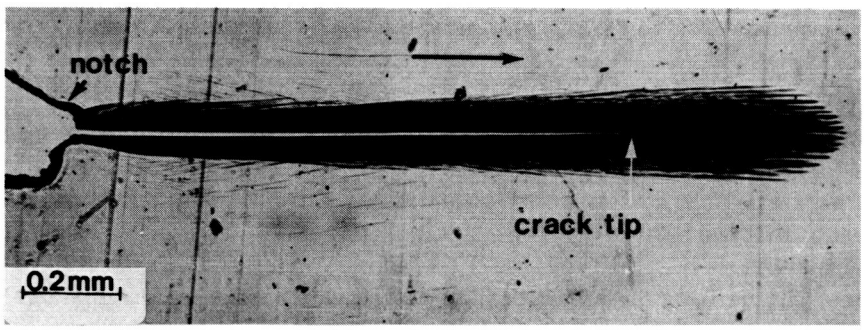


Fig. II.3 An optical micrograph displaying the Crazed Zone (CZ) surrounding the crack tip in PS.

Choosing a cartesian coordinate system with the origin at the crack tip (Fig. II.1), one can express the SIF as follows

$$K^{eff} = \frac{1}{\sqrt{\pi L}} \int_{-L}^{0} G(x_1)p(x_1)\, dx_1 \tag{II.10}$$

Here $L$ is the length of the main crack; $G(x_1)$ is the Green's function for the SIF due to a dipole unit force applied at $x_1$. In case of a crack in a single edge notch (SEN) specimen under mode I loading, $G(x_1)$ is given in [II.10]. The term $p(x_1)$ is the traction at the line of the main crack caused by the external load in combination with the MA interacting with the crack, i.e.,

$$p(x_1) = [\underset{\sim}{\sigma}_\infty + \underset{\sim}{\sigma}_\xi(x_1)]\underset{\sim}{n} \tag{II.11}$$

where $n$ is the unit normal vector to the main crack face. Thus the total (effective) SIF is naturally decomposed into a sum of the conventional SIF $K_o$ due to the externally applied load and the SIF $K_A$ due to the MA, i.e.,

$$K^{eff} = K_o + K_A \tag{II.12}$$

where

$$K_A = \frac{1}{\sqrt{\pi L}} \int_{-L}^{0} G(x_1)\underset{\sim}{\sigma}_A(\underset{\sim}{x}_1)\underset{\sim}{n}_x \, dx_1 \tag{II.13}$$

$\underset{\sim}{\sigma}_A$ is the stress due to the entire MA expressed by Eq. (II.8). The SIF $K_A$ is then given by

$$K_A = \frac{1}{\sqrt{\pi L}} \int_{-L}^{0} G(x_1) \int_{V_A} \underset{\sim}{\rho}(\underset{\sim}{\xi})F(\underset{\sim}{\xi},\langle \underset{\sim}{n}_\xi \rangle, x_1) \, d\underset{\sim}{\xi}dx_1 \tag{II.14}$$

$\underset{\sim}{\rho}(\underset{\sim}{\xi})$ is the microcrack opening density defined by Eq. (II.6) and $F(\xi, n(\xi), x_1)$ is $T_x[\Phi(\xi), \langle \underset{\sim}{n}_\xi \rangle, x]n_x$ at $x_2 = 0$.

In the case considered, i.e., the crazes are parallel to the main crack, $\langle \underset{\sim}{n}_\xi \rangle$ is the unit vector perpendicular to the main crack for all points $(\xi_1, \xi_2)$. Then the function $F(\xi, \langle \underset{\sim}{n}_\xi \rangle, x_1)$ in Eq. (II.14) can be written as (see Appendix)

$$F(\xi_1,\xi_2,x_1) = \frac{E}{4\pi}\left[\frac{(\xi_1 - x_1)^4 + 6(\xi_1 - x_1)^2\xi_2^2 - 3\xi_2^4}{\left[(\xi_1 - x_1)^2 + \xi_2^2\right]^3}\right] \tag{II.15}$$

where $E$ and $\nu$ are Young's modulus and Poisson's ratio, respectively. In addition, we assume that the MA size at the vicinity of the main crack tip is small with respect to the main crack length as well as with the distances from the specimen edges. Hence the second Green's tensor for an infinite plane (Eq. (II.2)) can be employed to approximate the second Green's tensor for the considered boundary value problem.

It is useful to introduce the Green's function $G_{SIF}$ for the SIF due to a unit discontinuity at the point $(\xi_1,\xi_2)$ normal to a line parallel to the main crack. Using Eqs. (II.14) and (II.15) and dimensionless coordinates $x_1'$, $\xi_1'$ and $\xi_2'$ representing $x_1$, $\xi_1$ and $\xi_2$ normalized by the crack length L, respectively, we obtain

$$G_{SIF}(\xi_1',\xi_2') = \frac{L}{\sqrt{\pi L}}\int_{-1}^{0} G(X_1)F(\xi_1',\xi_2',x_1')\,dx_1' \tag{II.16}$$

Depending on the location of the discontinuity $(\xi_1,\xi_2)$ $G_{SIF}$ can be positive or negative. A positive $G_{SIF}$ reflects an amplifying effect of the discontinuity, while a negative $G_{SIF}$ indicates shielding. A plot of the contours of equal values of the $G_{SIF}$ near the crack tip is shown in Fig. II.4. The contours are calculated using a numerical integration of Eq. (16) for $L/B = 0.5$. We note that this plot is very similar to the one obtained by Shiue and Lee [II.1] using the energy method for the case of a normal strain dislocation dipole. Rose [II.2] and Rubinstein [II.11] also reported similar results. The effect of a microcrack is symmetric with respect to the crack line. The border line between the amplification and shielding is a curve which

approaches the origin at an angle of about 69°. Apparently, the amplification

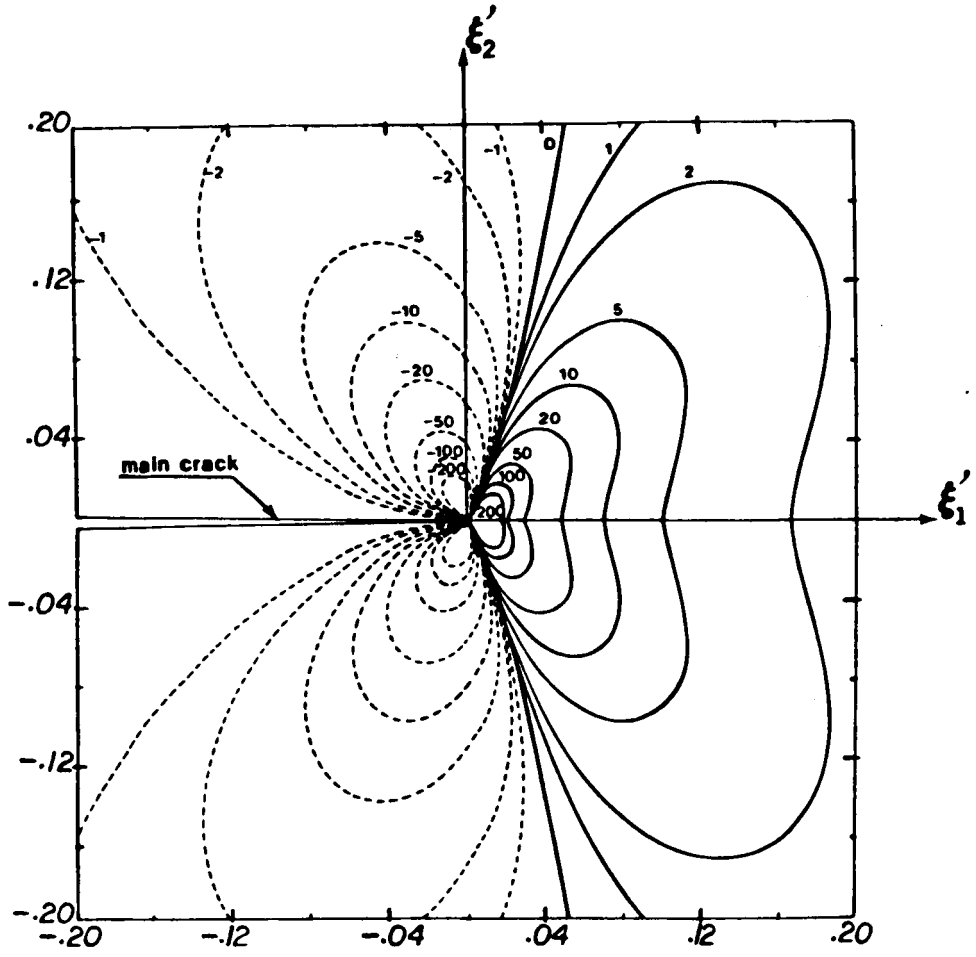


Fig. II.4 Contours of equal level of Green's function $G_{SIF}$ for the SIF $K_A$ due to a unit discontinuity, normalized by $10^5\ E\sqrt{\pi L}/b_o\omega$. $\xi_1'$ and $\xi_2'$ are the coordinates of the discontinuity, normalized by the length of the crack L. Here L/B = 0.5.

zone for mode I loading is located ahead of the crack tip.

In the considered case of an array of horizontal crazes [II.9], the only detectable non-zero component of the vector of craze opening density $\underset{\sim}{c}(\xi)$ is the vertical component $c_2(\xi)$, which is a product of craze opening $b_2(\xi)$ and the craze density $\rho(\xi)$. The latter is the total length of the craze middleline per unit area. This parameter has been studied by Botsis, et al., by means of optical microscopy [II.9]. An example of equal craze density con-

tours taken from [II.9] is shown in Fig. II.5. Using these data we employ an exponential-type approximation of the craze distribution

$$c_2(\underset{\sim}{\xi}) = b_o \rho_o \begin{cases} e^{-a_{k\ell}\bar{\xi}_k\bar{\xi}_\ell} & \xi_1 \geq 0 \\ e^{-a_{k\ell}\bar{\xi}_k\bar{\xi}_\ell}\Big|_{\xi_1=0} & \xi_1 \leq 0 \end{cases} \qquad \text{(II.17)}$$

$$k, \ell = 1,2; \quad \bar{\xi}_1 = \xi_1/\ell_a \; ; \quad \text{and} \quad \bar{\xi}_2 = \xi_2/w$$

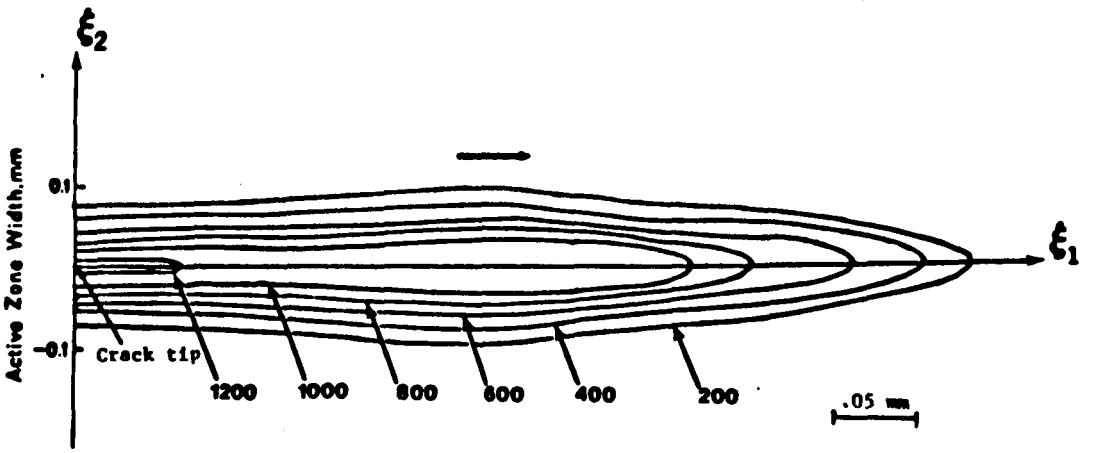


Fig. II.5 Contours of equal craze density in $mm^2/mm^3$ [II.9] for crack length L = 1.9 mm.

where $\ell_a$ and $w$ are the length and the width of the crazing zone (CZ) ahead of the crack tip, respectively. $\rho_o$ is the maximum craze density at the crack tip estimated as 1400 $mm^2/mm^3$ and $b_o$ is the average of the craze openings $b_2(\xi)$. The coefficients $a_{k\ell}$ are evaluated from the craze density measurement [II.9] and found to be

$$a_{k\ell} = \begin{bmatrix} 1.07 & -0.8 \\ -0.8 & 5.5 \end{bmatrix}$$

The overall effect of the CZ can be readily evaluated employing $G_{SIF}$ of Eq. (II.16) and the measured craze opening density $\underset{\sim}{c}(\xi)$ approximated by Eq. (II.17)

$$K_A = \int_{V_A} G_{SIF} \underset{\sim}{c}(\underset{\sim}{\xi})\, d\underset{\sim}{\xi} \qquad (II.18)$$

In the example considered, the following parameters are taken from [II.9]: crack length = 1.9 mm in a SEN specimen of 20 mm width, Young's modulus E = 2.2 GPa, Poisson's ratio $\nu = 0.3$, and the applied stress $\sigma_\infty$ is equal to 16 MPa. In this case $K_o$ = 1,378 kN/m$^{3/2}$ and $K_A$ is found to be $-1128 \times 10^6\ b_o$ kN/m$^{5/2}$, in which $b_o$ stands for an average craze opening in m upon load application. Since the latter was not measured, we use it as an adjustable parameter. Apparently, the total SIF $K^{eff}$ vanishes when $b_o = 1.22 \times 10^{-6}$ m. The value of 1 to $2 \times 10^{-6}$ m for craze openings under load seems quite realistic, thus suggesting an alternative to the well-known Dugdale-Barenblatt proposition [II.12,13], i.e., $K^{eff} = 0$ due to craze zone surrounding the crack.

## 5. Conclusion

The proposed crack tip analysis is essentially based on experimental measurements of the discontinuities and/or a discontinuity density. Then parameters such as SIF, energy momentum tensor and energy release rates can be evaluated by straightforward calculations based on the double layer potential technique.

The semi-empirical method can be also employed for stress analysis of crack damage interaction in non-polymeric (non-transparent) materials. With this in mind, various polymers and their blends may be selected to serve two purposes: a) mimicking brittle as well as ductile response to stress concentration at the crack tip and and b) to allow an observation and measurements of the discontinuity.

**ACKNOWLEDGEMENTS**

The authors are grateful to Dr. Shaofu Wu for corrections in computations.

**REFERENCES**

[II.1] S. Shiue and S. Lee, Engineering Fracture Mechanics, 22 (1985), 1105-1115.

[II.2] L. R. Rose, International Journal of Fracture, 31 (1986), 233-242.

[II.3] M. Kachanov, International Journal of Solids and Structures, 23 (1987) 23-43.

[II.4] R. G. Hoagland and J. D. Embry, Journal of the American Ceramic Society, 66 (1980) 404-410.

[II.5] S. K. Kanaun, in Elastic Media with Microstructure (ed. I. A. Kunin), Vol. 2, Chapter 7, Springer, Berlin (1983).

[II.6] A. Chudnovsky and M. Kachanov, Letters in Applied Engineering Science, 21 (1983) 1009-1018.

[II.7] A. Chudnovsky, A. Dolgopolsky and M. Kachanov, in Advances in Fracture Research, Proceedings IFC6, Vol. 2, ed. S. R. Valluri, et al., Pergamon Press, Oxford (1984) 825-832.

[II.8] A. Chudnovsky, A. Dolgopolsky and M. Kachanov, International Journal of Solids and Structures, 23 (1987) 1-21.

[II.9] J. Botsis, A. Chudnovsky and A. Moet, International Journal of Fracture 33 (1986) 263-276.

[II.10] H. Tada, P. C. Paris and G. R. Irwin, The Stress Analysis of Cracks Handbook, Del Research Corporation, Hellertown, PA (1973) 2.27.

[II.11] A. A. Rubinstein, Journal of Applied Mechanics, Transactions of the ASME, 53 (1986) 505-510.

[II.12] D. S. Dugdale, Journal of the Mechanics and Physics of Solids, 8 (1960) 100.

[II.13] G. I. Barenblatt, Advances in Applied Mechanics, 7 (1962) 55.

## APPENDIX

The displacement generated by a microcrack is

$$u_i(x) = \int_\omega b_j(\xi)\,\Phi_{ij}(\xi,x)\,d\xi \tag{A1}$$

In case of an horizontal microcrack $b_1(\xi) = 0$ and therefore

$$u_1(\underset{\sim}{x}) = \int_\omega b_1(\xi)\,\Phi_{12}(\underset{\sim}{\xi},\underset{\sim}{x})\,d\xi$$

$$u_2(\underset{\sim}{x}) = \int_\omega b_2(\xi)\,\Phi_{22}(\underset{\sim}{\xi},\underset{\sim}{x})\,d\xi \tag{A2}$$

For plane stress, the stress-displacement relation is given by

$$\sigma_{22}(x) = \frac{E}{(1-\nu^2)}\,[u_{2,2}(\underset{\sim}{x}) + \nu u_{1,1}(\underset{\sim}{x})] \tag{A3}$$

Therefore, the stress operator applied to the second Green's tensor $\Phi(\xi,x)$ gives

$$T_x[\underset{\sim}{\Phi}(\underset{\sim}{\xi},\underset{\sim}{x})] = \frac{E}{(1-\nu^2)}\,[\Phi_{22,2}(\underset{\sim}{\xi},\underset{\sim}{x}) + \nu\Phi_{12,1}(\underset{\sim}{\xi},\underset{\sim}{x})] \tag{A4}$$

From Eq. (2) in the text, we write the second Green's tensor as

$$\Phi_{12}(\underset{\sim}{\xi},\underset{\sim}{x}) = -\frac{(1+\nu)}{4\pi R^2} - \left[\frac{1-\nu}{1+\nu}\,R_1 + 2\,\frac{R_1 R_2^2}{R^2}\right]$$

$$\Phi_{22}(\underset{\sim}{\xi},\underset{\sim}{x}) = \frac{(1+\nu)}{4\pi R^2}\left[\frac{1-\nu}{1+\nu}\,R_2 + 2\,\frac{R_2^3}{R^2}\right] \tag{A5}$$

where $R_1 = \xi_1 - x_1$, $R_2 = \xi_2 - x_2$ and $R^2 = R_1^2 + R_2^2$ The derivatives with respect to $x_1$ and to $x_2$ gives

$$\Phi_{12,1}(\underset{\sim}{\xi},\underset{\sim}{x}) = \frac{(1+\nu)}{4\pi R^6}\left[\frac{1-\nu}{1+\nu}\left(R_1^4 - 6R_1^2R_2^2 + \frac{1-3\nu}{1+\nu}\right)R_2^4\right] \tag{A6}$$

$$\Phi_{22,2}(\underset{\sim}{\xi},\underset{\sim}{x}) = \frac{(1+\nu)}{4\pi R^6}\left[\frac{1-\nu}{1+\nu}\left(R_1^4 + 6R_1^2R_2^2 - \frac{3+\nu}{1+\nu}\right)R_2^4\right]$$

Therefore, Eq. (A4) becomes, for $x_2 = 0$, as

$$F(\xi_1,\xi_2,x_1) = \frac{E}{4\pi R^6}\,(R_1^4 + + 6R_1^2R_2^2 - 3R_2^4)$$

## III. EXPANSION OF THE ACTIVE ZONE

The requirement of self-similarity hypothesis (Part I) has two implications: (i) the evolution of the active zone can be approximated by four elementary moments, namely, translation and rotation as a rigid body, expansion and distortion. (ii) It allows to express the active parts of the corresponding driving forces in the form of the J, L, M and $N_{ij}$ integrals, respectively [III.1].

Crack propagation which coincides with the translation of the active zone is a relatively fast process. The CL theory derives the kinetic equation for active zone translation by employing the principle of minimum entropy production [III.1,2]. On the other hand, active zone deformation and rotation result from slow processes of damage growth.

On the basis of experimental observations, various propositions can be made with respect to the constitutive equations for expansion, distortion and rotation of the active zone. Herein we concentrate on the expansion of the active zone only.

In this respect we have examined two candidates for constitutive relations; Onsanger's type linear relation

$$\dot{e} = LX_{exp} \tag{III.1}$$

and Arrhenius type exponential relation

$$\dot{e} = C_1 \exp [-C_2 X_{exp}] \tag{III.2}$$

between the rate of expansion $\dot{e}$, and the corresponding force $X_{exp}$. The coefficients $L[\text{sec}\cdot\text{Joules}^{-1}]$ (Eq. (III.1)), $C_1[\text{sec}]$ and $C_2[\text{Joules}^{-1}]$ (Eq. (III.2)) are obtained from linear regression analysis.

Under the assumption of homogeneous deformation within the active zone, the rate of expansion $\dot{e}$ with the crack tip as the origin is

$$\dot{e} = \frac{1}{2}\left(\frac{\dot{w}}{w} + \frac{\dot{\ell a}}{\ell a}\right)$$

where $w$ and $\ell a$ are the width and length of the active zone, respectively (Fig. I.1). The force $X_{exp}$ is expressed as the difference between active and resistive parts, i.e.,

$$X_{exp} = M - \gamma R_o \tag{III.3}$$

Here $M$ is the energy release rate due to expansion of the active zone, $\gamma$ is the specific enthalpy of damage and $R_o$ is the resistance moment of the active zone associated with the expansion. Both $M$ and $R_o$ are approximated as

$$M \cong \frac{1}{2}\,\alpha J_1 \ell a \tag{III.4}$$

$$R_o \cong \langle \rho_o \rangle A \tag{III.5}$$

where $J_1$ is the energy release rate due to translation of the active zone, $\ell a$ is the length of the active zone and $\alpha$ is a dimensionless coefficient with $0 < \alpha \leq 1$. $\langle \rho_o \rangle$ is the average damage density within the active zone and $A$ its area.

Analysis of CL stability has shown that the critical energy release rate $A_{1c}$, can be expressed as the product of the specific enthalpy of damage $\gamma^*$, and the resistance moment at critical propagation, namely, $A_{1c} = \gamma^* R_{1c}$. This process is a manifestation of mainly new damage nucleation. Thus $\gamma^*$ is directed related to the corresponding specific energy (i.e., energy of nucleation of new damage). On the other hand, $\gamma$ which appears in Eq. (III.3)

corresponds mainly to the energy of relative slow process which follows the nucleation. Furthermore, it is well recognized that the difference between the energy of new phase nucleation and the energy of phase growth is essential [III.3]. Accordingly, it is expected that $\gamma^*$ is significantly greater than $\gamma$.

For our model material, $\gamma^*$ has been found to be of the order of 30 $J/m^2$ [III.4]. An experimental method to evaluate $\gamma$ is being developed. To compare the two candidates (Eqs. (III.1) and (III.2)) for constitutive equations for active zone expansion, we take $\gamma$ to be 10% of $\gamma^*$.

Fracture propagation kinetics are observed under two different fatigue load histories. Whereas the frequency and load ratio were the same, the level of mean stress is 16.0 MPa and 10.7 MPa, respectively.

Analysis of the experimental results according to Onsanger relationship (Eq. (III.1)) resulted in two different values of the kinetic coefficient L, namely, $L = 0.98 \times 10^{-2}$ sec $\cdot$ joules$^{-1}$ for the first experiment and $L = 0.68 \times 10^{-2}$ sec$\cdot$joules$^{-1}$ for the second experiment. In addition, in both cases the coefficient of correlation in the linear regression analysis, in the $\dot{e}$, $X_{exp}$ plane, was low, regardless of the value of the parameter $\alpha$.
This suggests that simple Onsanger relationship is not adequate.

The solid lines in Fig. III.1 represent the right-hand side of (III.2). The data points are measurements of the rate of expansion of the active zone. The correlation coefficient for both set of data was of the order of 0.9 and the pre-exponent parameter $C_1$ was $1.12 \times 10^{-3}$ sec and $0.34 \times 10^{-3}$ sec, respectively. On the other hand, the coefficient $C_2$ was found to be the same for both experiments regardless of the parameter $\alpha$. If an Arrhenius type constitutive relationship was to describe the expansion rate, $C_2$ should be the same in this case since both experiments were performed under different load

levels and the same temperature. This is very strong evidence that Eq. (III.2) could be adopted to describe the expansion rate of the active zone. In order, however, to unquestionably assess the applicability of an Arrhenius type kinetic equation for active zone expansion, experiments with different loading rates and temperatures should be available.

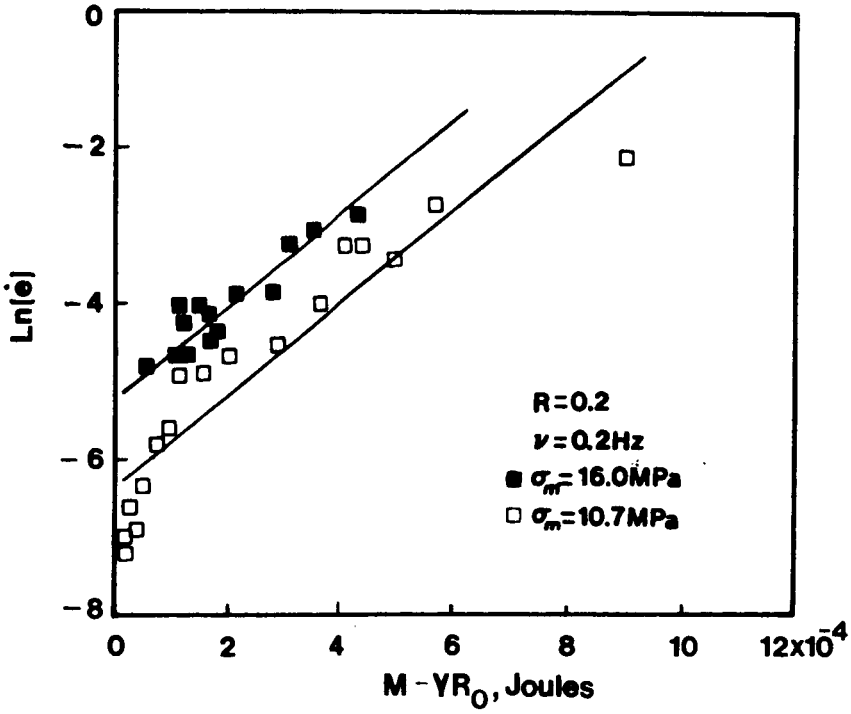


Fig. III.1 Rate of expansion as a function of the expansional thermodynamic force for two levels of mean stress. Note that the lines are parallel.

## REFERENCES


[III.1] A. Chudnovsky, 'Crack Layer Theory,' NASA Report 174634.

[III.2] A. Chudnovsky, 'Crack Layer Theory,' Journal of Applied Mechanics, to appear.

[III.3] O. H. Wyatt and D. Dew-Hughes, 'Metals, Ceramics and Polymers,' Cambridge University Press, London, 1974.

[III.4] J. Botsis, A. Chudnovsky and A. Moet, Int. J. Fracture, 33 (1987) 277.

NASA
National Aeronautics and Space Administration

# Report Documentation Page

| 1. Report No. | 2. Government Accession No. | 3. Recipient's Catalog No. |
|---|---|---|
| NASA CR-182120 | | |

| 4. Title and Subtitle | 5. Report Date |
|---|---|
| On Governing Equations for Crack Layer Propagation | April 1988 |
| | 6. Performing Organization Code |

| 7. Author(s) | 8. Performing Organization Report No. |
|---|---|
| A. Chudnovsky and J. Botsis | None |
| | 10. Work Unit No. |
| | 535-07-01 |

| 9. Performing Organization Name and Address | 11. Contract or Grant No. |
|---|---|
| University of Illinois at Chicago Circle<br>Dept. of Civil Engineering, Mechanics, and Metallurgy<br>Chicago, Illinois 60637 | |
| | 13. Type of Report and Period Covered<br>Contractor Report<br>Final |
| 12. Sponsoring Agency Name and Address | 14. Sponsoring Agency Code |
| National Aeronautics and Space Administration<br>Lewis Research Center<br>Cleveland, Ohio 44135-2191 | |

15. Supplementary Notes

Project Manager, John L. Shannon, Jr., Structures Division, NASA Lewis Research Center.

16. Abstract

Results of analysis on damage distribution of a crack layer, in a model material, supported the self-similarity hypothesis of damage evolution which has been adopted by the crack layer theory. On the basis of measurements of discontinuity density and the double layer potential technique, a solution to the crack damage interaction problem has been developed. Evaluation of the stress intensity factor illustrated the methodology. Analysis of experimental results showed that Arrhenius type constitutive relationship described very well the expansion of the active zone of a crack layer.

| 17. Key Words (Suggested by Author(s)) | 18. Distribution Statement |
|---|---|
| Fatigue; Damage; Crack layer; Fracture mechanics; Crack shielding; Microcracks; Double layer potential | Unclassified - Unlimited<br>Subject Category 39 |

| 19. Security Classif. (of this report) | 20. Security Classif. (of this page) | 21. No of pages | 22. Price* |
|---|---|---|---|
| Unclassified | Unclassified | 26 | A03 |



*For sale by the National Technical Information Service, Springfield, Virginia 22161